Journal of Quantitative Spectroscopy & Radiative Transfer 113 (2012) 976–990

Contents lists available at SciVerse ScienceDirect

Journal of Quantitative Spectroscopy & Radiative Transfer

journal homepage: www.elsevier.com/locate/jqsrt

Semiclassical calculations of half-widths and line shifts for transitions in the 30012←00001 and 30013←00001 bands of CO_2, I: Collisions with N_2

Robert R. Gamache [a,b,*], Julien Lamouroux [a,b], Anne L. Laraia [a,b], Jean-Michel Hartmann [c], Christian Boulet [d]

[a] University of Massachusetts School of Marine Sciences, 1 University Avenue, Lowell, MA 01854-5045, USA
[b] Department of Environmental, Earth, and Atmospheric Sciences, University of Massachusetts Lowell, 1 University Avenue, Lowell, MA 01854-5045, USA
[c] Laboratoire Interuniversitaire des Systèmes Atmosphériques, CNRS (UMR 7583), Université Paris Est Créteil, Université Paris Diderot, Institut Pierre-Simon Laplace, Université Paris Est Créteil, 94010 Créteil Cedex, France
[d] Institut des Sciences Moléculaires d'Orsay (ISMO;UMR 8214), CNRS, Univ. Paris-Sud, Bat. 350, Campus d'Orsay, 91405 Orsay Cedex, France

ARTICLE INFO

Available online 18 February 2012

Keywords:
Half-width
Line shift
Temperature dependence of the half-widths
CO_2–N_2

ABSTRACT

Calculations of the half-width, its temperature dependence, and the line shift are made for the rotational states $J=0$–120 for two of the Fermi-tetrad bands (30012←00001 and 30013←00001) of CO_2 perturbed by N_2. The calculations employ the semi-classical complex Robert–Bonamy method with no *ad hoc* scaling, J-dependent or otherwise, and an intermolecular potential (IP) comprised of an electrostatic part, an atom–atom part, and an isotropic London dispersion part. The averaging over the impact parameter b and relative speed v are explicitly carried out. Many interesting features about CO_2 as the radiating molecule are elucidated. Effects of the trajectory model, the order of the expansion of the atom–atom component of the potential, and the inclusion of the imaginary terms are studied. It is shown that the results are very sensitive to the intermolecular potential. The final IP parameters give results that demonstrate excellent agreement with measurement for the three line shape parameters studied in this work.

1. Introduction

Carbon dioxide is the second strongest absorber of infrared radiation in the Earth's atmosphere after water vapor [1]. However, unlike water vapor, which has a residence time in the atmosphere of roughly 9 days, CO_2 lifetime in the terrestrial atmosphere is about 120 years. Because of the ability of carbon dioxide to absorb IR radiation and its long lifetime it has become the standard by which other molecules are gauged in global climate change. CO_2's concentration has been monitored by direct measurement since 1957 [2,3] and proxy records go back hundreds of thousands of years [4]. The current average concentration of ~390 ppm is larger than it has been in at least 650 thousand years [4,5]. The concentration of CO_2 in the Earth's atmosphere began rising abruptly after the industrial revolution and this increased concentration of CO_2 is thought to be of anthropogenic origin [6]. To address this question a number of measurement programs are devoted to measuring CO_2 to high precision in the Earth's atmosphere. There are several satellite-based instruments that are making remote sensing measurements of CO_2 in the atmosphere. In the mid-infrared region the Atmospheric Infrared Sounder (AIRS) [7] on board the AQUA satellite [8] and the Infrared Atmospheric

* Corresponding author at: Department of Environmental, Earth, and Atmospheric Sciences, University of Massachusetts Lowell, 1 University Avenue, USA. Tel.: +1 978 934 3904; fax: +1 978 934 3069.
E-mail address: Robert_Gamache@uml.edu (R.R. Gamache).

0022-4073/$ - see front matter © 2012 Elsevier Ltd. All rights reserved.
doi:10.1016/j.jqsrt.2012.02.014

Sounder Interferometer (IASI) [9] onboard the METOP-A satellite [10]. The Japanese launched the Greenhouse Gases Observing Satellite (GOSAT) [11] in 2009, which targets near-IR transitions of carbon dioxide particularly in the 1.6 μm region. Also in 2009, the Jet Propulsion Laboratory's Orbiting Carbon Observatory (OCO) mission [12] failed to reach orbit; however, NASA has stated that due to the importance of the mission OCO-2 will be launched in 2013. OCO-2 will need spectroscopic parameters with uncertainty of less than 0.3%, placing strong demands on the spectroscopic community. The additional complications of line mixing for CO_2 [13] and high temperature applications such as Venus [14] are of concern for modeling CO_2 in planetary atmospheres.

The 2008 version of the HITRAN database [1] contains 314 919 transitions for the nine isoptopologues of carbon dioxide; the principal isotopologue, $^{12}C^{16}O_2$, accounting for 128 170 of these transitions. Some of the instruments, GOSAT and OCO, are designed to measure in the range 4250–7000 cm^{-1} region in order to support atmospheric remote sensing, however, GOSAT band 4 of the TANSO-FTS covers the ~700–1800 cm^{-1} region. It is certainly impractical to attempt to measure so many transitions at the number of pressures and temperatures needed for application to planetary atmospheres. Theory can be an attractive alternative if the theory can meet the precision needs of the spectroscopic and remote sensing community [15–17].

There have been a number of previous calculations of broadening of CO_2 by N_2, O_2, air, and CO_2. Yamamoto et al. [18] used the theory of Anderson–Tsao–Curnutte (ATC) [19–21] to calculate nitrogen- and self-broadening of carbon dioxide for four bands in the 15 and 4.3 μm region. Bouanich and Brodbeck [22] made calculations of N_2-, O_2-, H_2-, and CO_2-broadening of CO_2 using ATC theory adding the hexadecapole–dipole, hexadecapole–quadrupole, hexadecapole–octupole, and hexadecapole–hexadecapole interaction terms to the electrostatic intermolecular potential and noted better agreement with measurement. The ATC theory calculations have the cutoff problem, straight line trajectories, and only considering the electrostatic component of the internuclear potential. In 2000 Bykov et al. [23] made ATC calculations for N_2- and O_2-broadening of CO_2 where the resonance functions have an *ad hoc J*-dependent scaling with 2 fitting parameters. They reported the air-broadened half-widths, line shifts, and the temperature dependence for both parameters for the ν_3 band. Arié et al. [24] made calculations of oxygen- and air-broadening of CO_2 using the real components of the formalism of Robert and Bonamy (RB) [25], which eliminated the cutoff problem, used the parabolic model of Robert and Bonamy for the trajectory calculation, the mean-relative thermal velocity approximation, and considered an atom–atom component in the intermolecular potential. This work was followed by a series of calculations using the RB method for CO_2 broadened by a number of different perturbing gases [26–29], with several studies evaluating the velocity integral [30,31]. However, all of the calculations made, ATC or RB, used only the real components of the theory and the moments of the molecules (quadrupole, hexadecapole, etc.) and atom–atom parameters, when used, were scaled. The moments of these molecules are reasonably well known and the scaling was needed to give agreement with the measurements.

The exponential form in the Robert–Bonamy theory that comes from the application of the linked cluster theorem [32] results in the half-width and line shift depending on both the real and imaginary components of the scattering matrix. (Note, in ATC theory the half-width and line shift are given by the real and imaginary parts of the scattering matrix, respectively.) It has been shown that the imaginary components can contribute significantly to the half-width for certain collision systems [33–38]. The effect on the half-widths varies as a function of transition and perturber but can be as much as 25%. The change is almost always in the direction of better agreement with experiment. It is also known that the addition of the atom–atom potential not only improves agreement with measurement, it is essential for weak collision systems [35,38–40]. Some recent work [41,42] has shown that the expansion of the atom–atom potential necessary for convergence is greater than that used in the previous calculations. The influence of the collision trajectories is also now better understood [43–46]. Because the half-width and the line shift come from a single calculation in the complex RB formulation, the complex calculation imposes a constraint on the intermolecular potential to yield both parameters at once. Since the potential is independent of temperature, results of the calculations can be reported at several temperatures to determine the temperature dependence of the half-width and line shift.

This work presents calculations of the half-width, its temperature dependence, and the line shift of carbon dioxide perturbed by N_2 from a single intermolecular potential. As will be shown below the results are strongly dependent on the potential. The goal was that a single set of potential parameters will yield half-widths, their temperature dependence, and line shifts that agree well with measurement.

2. Complex Robert–Bonamy formalism

Robert–Bonamy theory [25], in its complex form (CRB), was developed using the resolvent operator formalism of Kolb and Griem [47], Baranger [48], and Griem [49] (KBG). Appling linked-cluster techniques [32] to the KBG formalism leads to developments [25,50,51] which eliminate the awkward cutoff procedure that characterized earlier theories [19–21]. With the inclusion of a short-range (Lennard–Jones 6–12 [52]) atom–atom component to the intermolecular potential the CRB formalism can be applied to close collision systems. This short-range component is essential for a proper description of pressure broadening, especially in systems where electrostatic interactions are weak [39,53–55]. (The notion of strong and weak collisions follows the definition of Oka [56].)

In the CRB formalism, the half-width, γ, and line shift, δ, of a ro-vibrational transition $f \leftarrow i$ are given by minus the imaginary part and the real part, respectively, of the diagonal elements of the complex relaxation matrix.

In computational form, they are usually expressed in terms of the Liouville scattering matrix [48,57]

$$\gamma_{f\leftarrow i} = \frac{n_2}{2\pi c}\sum_{J_2}\langle J_2|\rho_2|J_2\rangle \int_0^\infty v f(v)\,dv \times \int_0^\infty 2\pi b[1-\cos\{S_1+\mathrm{Im}(S_2)\}\,e^{-\mathrm{Re}(S_2)}]\,db \quad (1a)$$

$$\delta_{f\leftarrow i} = \frac{n_2}{2\pi c}\sum_{J_2}\langle J_2|\rho_2|J_2\rangle \int_0^\infty v f(v)\,dv \int_0^\infty 2\pi b \sin\{S_1+\mathrm{Im}(S_2)\}\,e^{-\mathrm{Re}(S_2)}\,db \quad (1b)$$

where v is the relative velocity, b is the impact parameter, ρ_2 and n_2 are the density operator (its matrix element in the preceding equations giving the relative population) and number density of perturbers. S_1 and S_2 are the first and second order terms in the successive expansion of the Liouville scattering matrix.

2.1. Intermolecular potential

The potential used in the CRB codes consists of electrostatic components, an atom–atom component [39,58], and isotropic induction and dispersion components. The isotropic component of the atom–atom potential is used as the starting point to define the trajectory of the collision by using the Robert–Bonamy parabolic trajectory (PT) approximation or by solving Hamilton's equations.

The atom–atom potential is given by the sum of pairwise Lennard–Jones 6–12 interactions [52] between atoms of the radiating molecule and the perturbing molecule, labeled 1 and 2 respectively,

$$V^{at-at} = \sum_{i=1}^{n}\sum_{j=1}^{m} 4\varepsilon_{ij}\left\{\frac{\sigma_{ij}^{12}}{r_{1_i,2_j}^{12}} - \frac{\sigma_{ij}^{6}}{r_{1_i,2_j}^{6}}\right\}. \quad (2)$$

The subscripts 1_i and 2_j refer to the ith atom of molecule 1 and the jth atom of molecule 2, respectively, n and m are the number of atoms in molecules 1 and 2, respectively, and ε_{ij} and σ_{ij} are the Lennard–Jones or atom–atom parameters for the atomic pairs.

Gray and Gubbins [59,60], using the expansion of Sack [61] to express the atom–atom distance, $r_{1i,2j}$, in terms of the center of mass separation, R, have shown that the atom–atom potential can be expressed as a spherical tensor expansion

$$V = \sum_{\ell_1\ell_2}\sum_{\substack{n_1\\ \ell\ m_1m_2\\ m}}\sum_{w,q}\frac{U(\ell_1\ell_2\ell,n_1wq)}{R^{q+\ell_1+\ell_2+2w}} \times C(\ell_1\ell_2\ell,m_1m_2m)D^{\ell_1}_{m_1n_1}(\Omega_1)D^{\ell_2}_{m_20}(\Omega_2)Y_{\ell m}(\omega) \quad (3)$$

where $C(\ell_1, \ell_2, \ell; m_1, m_2, m)$ is a Clebsch–Gordan coefficient, $\Omega_1=(\alpha_1, \beta_1, \gamma_1)$ and $\Omega_2=(\alpha_2, \beta_2, \gamma_2)$ are the Euler angles describing the molecular fixed axis relative to the space fixed axis, $\omega=(\theta,\phi)$ describes the relative orientation of the centers of mass. The powers w and q (integers) depend upon the interaction, and the coefficients $U(\ldots)$ are given in Refs. [34] or [59]. Since the expansion in $(1/R)$ must be truncated, sufficient order must be chosen to ensure the convergence of calculated half-widths and line shifts (see discussion below). Here the atom–atom formulation of Neshyba and Gamache [58] is used.

With respect to the atom–atom potential, three points should be emphasized:

(1) The atom–atom potential as expressed by Eq. (3) can be understood by two different labeling schemes. The first is defined by the tensorial *ranks* ℓ_1 and ℓ_2, which determine the symmetry of the interaction [59,60]. The second is defined by the sum $\ell_1+\ell_2+2w$ [61,62], which is called the *order* of the expansion. When discussing the potential the nomenclature adopted is *orde*r, ℓ_1, ℓ_2: thus an atom–atom potential expanded to 12 4 2 is one that is *order*=12, ℓ_1=4, and ℓ_2=2. The expansion and convergence are discussed below.

(2) The $\ell_1=\ell_2=0$ components of the atom–atom potential define an isotropic part, which in general is comprised of terms of the form $1/R^6$, $1/R^8$, $1/R^{10}$, etc. The isotropic terms can be fit for convenience to an effective isotropic Lennard–Jones (*L–J*) 6–12 potential,

$$V^{iso} = 4\varepsilon\left[\left(\frac{\sigma}{R}\right)^{12} - \left(\frac{\sigma}{R}\right)^{6}\right]. \quad (4)$$

The isotropic components are used in the calculation to define the intermolecular trajectory.

(3) The remaining atom–atom potential terms have nonzero ℓ_1 or ℓ_2 (anisotropic), and have labels similar to the electrostatic interaction labels. Thus the $\ell_1=2$ and $\ell_2=2$ interaction is designated as an "atom–atom quadrupole–quadrupole" term. Note, these are symmetry appellations only, and the powers of R that arise in Eq. (3) are quite different than those for the electrostatic terms [37].

The vibrational dephasing term, S_1, which appears in the imaginary part of Eqs. (1), depends on the difference between the average values of the isotropic component of the potential within the final and initial vibrational levels. For pure rotational transitions the S_1 term is zero. In the present work, it will be assumed that it can be written only in terms of the vibrational dependence of the isotropic dispersion component in CO_2 in $1/R^6$, neglecting therefore the vibrational dependence of all the other components. Within the Unsöld approximation the London dispersion potential is given by

$$V_{iso}^{dispersion} \equiv \frac{C_6^{0,0}}{R^6} \simeq -\frac{3}{2}\frac{I_1I_2}{I_1+I_2}\frac{\alpha_1\alpha_2}{R^6} \quad (5)$$

where α_k and I_k are the polarizability and ionization potential for carbon dioxide (k=1) and nitrogen (k=2). It is the change in the polarizability of the radiating molecule (CO_2) with vibrational state that contributes to the half-width and line shift. The vibrational average value of the polarizability [63] in a given $|v\rangle$ vibrational state can be expressed as

$$\langle v|\alpha|v\rangle = \alpha_0 + a_1\left(n_1+\tfrac{1}{2}\right) + a_2\left(n_2+\tfrac{1}{2}\right) + a_3\left(n_3+\tfrac{1}{2}\right) \quad (6)$$

where n_1, n_2, and n_3 are the number of quanta in the v_1, v_2, and v_3 vibrational levels, α_0 is the polarizability at equilibrium, and a_1, a_2, and a_3 are the coefficients of the vibrational dependence of the polarizability. These coefficients are needed for the calculations. The determination of their values is discussed below.

The last terms to discuss are the second-order terms, S_2. These are the complex analog of those appearing in the ATC theory [19–21]

$$S_2(i,f,b,v) = S^*_{2,i2}(i,b,v) + S_{2,f2}(f,b,v) + S_{2,middle}(i,f,b,v) \quad (7)$$

where the notation is that of Anderson [20]. $S_{2,middle}$ has only a real component and is given by

$$S_{2,middle} = \frac{[J_i]^{1/2}[J_f]^{1/2}}{\hbar^2[J_2]} \sum_{J_{2'}} \sum_{\substack{\ell_1\ell_2 \\ n^a n^b}} D(\ell_1\ell_2, n^a n^b J_f J_{f'} J_2 J_{2'}) \times F^{\ell_1\ell_2}_{n^a n^b}(\omega_{2,\,2'})[J_{2'}]^{1/2}(-1)^{J+J_i+J_f+\ell} \begin{Bmatrix} J_i & J_i & \ell \\ J_f & J_f & 1 \end{Bmatrix}. \quad (8)$$

The other terms, called the "*outer*" terms in Anderson's notation, are complex functions and can be written in the form

$$S_{2,f2} = \frac{1}{2\hbar^2} \sum_{J_{2'}J_{f'}} \sum_{\substack{\ell_1\ell_2 \\ n^a n^b}} D(\ell_1\ell_2, n^a n^b J_f J_{f'} J_2 J_{2'}) F^{\ell_1\ell_2}_{n^a n^b}(\omega_{f2,f'2'}) \quad (9)$$

where $[J]=2J+1$, $\mathbf{n}=(n_1,n_2)$, $\omega_{2,\,2'}=(E_{J2'}-E_{J2})$, $\{\ldots\}$ is a Racah coefficient, and $\omega_{f2,f'2'}=(E_{f'}-E_f+E_{J2'}-E_{J2})$ with E_s being the energy of the state s; f' and f label the states of the radiating molecule (collisional transition $f\rightarrow f'$) and J_2' and J_2 label the states of the perturbing molecule (collisional transition $J_2\rightarrow J_2'$). $S_{2,i2}$ is obtained from Eq. (9) by replacing f with i. The F terms are the resonance functions for the real and imaginary terms [34,38]. The $D(\ldots)$ terms in Eqs. (8) and (9) are the reduced Liouville matrix elements for the internal states of the radiator and perturber. They are expressed in terms of reduced Hilbert-space matrix elements using the conventions of Gray and Gubbins [59] and are defined by

$$\langle J_1 K_1 M_1 | D^{\ell}_{m',m} | J_2 K_2 M_2 \rangle = (-1)^{M_1} \begin{pmatrix} J_1 & J_2 & \ell \\ M_1 & -M_2 & 1 \end{pmatrix} [J_1]^{1/2} \langle J_1 \| D^{\ell}_{*,m} \| J_2 \rangle, \quad (10)$$

which then gives

$$D(\ell_1\ell_2, n^a n^b J_f J_{f'} J_2 J_{2'}) = \langle J_f \| D^{\ell}_{*,n_1^b} \| J_{f'} \rangle \langle J_f \| D^{\ell}_{*,n_1^a} \| J_{f'} \rangle^* \langle J_2 \| D^{\ell}_{*,n_2^b} \| J_{2'} \rangle \langle J_2 \| D^{\ell}_{*,n_2^a} \| J_{2'} \rangle^*, \quad (11)$$

where J_f, J_2, etc. represent all the quantum numbers of the states. In general the wavefunctions can be expressed as a sum over Wigner D-matrices with coefficients τ_K, however, for CO_2 only the $K=0$ component of the wavefunction exist so states are proportional to the Wigner D-matrix, $D^J_{00}(\Omega)$, and the resulting reduced matrix elements are given by a Clebsch–Gordan coefficient.

3. Calculations

In this work CRB calculations were made for transitions in two of the Fermi-tetrad bands of CO_2 ($30012\leftarrow00001$ and $30013\leftarrow00001$) broadened by N_2. Note, the Fermi-tetrad bands are labeled using the notation [64] $30011\leftarrow00001$ ($3v_1+v_3$), $30012\leftarrow00001$ ($2v_1+2v_2+v_3$), $30013\leftarrow00001$ ($v_1+4v_2+v_3$) and $30014\leftarrow00001$ ($6v_2+v_3$). These calculations yield the half-width, γ, its temperature dependence, n, and the line shift, δ. The reason for choosing these bands is that they are being used in atmospheric remote sensing measurements and there are accurate measurements of these parameters as a function of m from the work of Devi et al. [65] (γ and δ) and Predoi-Cross et al. [31] (n values for CO_2–air). The intermolecular potential used in the calculations consists of the leading electrostatic components for the CO_2–N_2 collision system (quadrupole moment of CO_2 with the quadrupole moment of N_2), an atom–atom component expanded to *order* 20 with the ranks, ℓ_1 and ℓ_2, set to 4 based on the work of Ma et al. [41] and Gamache et al. [42], and the isotropic London dispersion vibrational dephasing term. Measurements of the quadrupole moment of carbon dioxide [59] yield values which range from -4.0 to roughly -4.6 in units of 10^{-26} esu. The value $\Theta_{zz}=-3.698\times10^{-26}$ esu is adopted in this work based on the measurements of Graham et al. [66] and a study of self-broadening of CO_2 [67]. The polarizability of carbon dioxide, 29.13×10^{-25} cm^3, is taken from Ref. [68] and the ionization potential, 13.77 eV, from Tanaka et al. [69]. The quadrupole moment of nitrogen ($\Theta_{zz}=-1.4\times10^{-26}$ esu) is from Mulder et al. [70]. The polarizability of nitrogen, 17.4×10^{-25} cm^3, is taken from Bogaard and Orr [71] and the ionization potential, 15.576 eV, from Lofthus [72].

The heteronuclear atom–atom parameters (the ε_{ij} and σ_{ij} of Eq. (2)) are usually determined using combination rules with homonuclear-atom–atom parameters, however, many different combination rules have been proposed [73] (and references therein), [74]. Good and Hope [75] have shown that the determination of ε using different combination rules lead to variations as large as ~15% and different references report the input (homonuclear) Lennard–Jones parameters for the same system with some ε values varying by 30% and the σ values by 5%. Also, values derived from viscosity data or virial data do not agree [76]; ε values can vary by as much as 69% and the σ values by 9%. These facts indicate caution should be used when using these procedures. Several studies have demonstrated that one can get a good set of atom–atom parameters by starting from coefficients determined using the combination rules given in Hirschfelder et al. [76] and then adjusting them to give results in better agreement with measurement [77–79]. For some systems relatively small changes in the atom–atom parameters can lead to much improved agreement with measurement (see Ref. [77] for details).

The coefficients of the vibrational dependence of the polarizability (see Eq. (6)) must also be determined. These coefficients can be estimated from measurements [80,81] or *ab initio* calculations [82]. However, Hartmann [83]

developed a simple empirical model to calculate shifts for CO_2–air and determined the coefficients by fitting to measurement. Hartmann's values were taken as a starting point to adjust the coefficients in the CRB calculations based on experimental determination of the coefficients.

Lastly, the *L–J* parameters (Eq. (4)) for the trajectory calculations must be adjusted.

Thus in the intermolecular potential the values of the N_2 quadrupole moment, ionization potentials, and polarizabilities are fixed at the best-measured values. The quadrupole moment of CO_2 is set to the value given above. The atom–atom parameters, the isotropic atom–atom parameters used in the trajectory calculations, and vibrational dependence of the polarizability coefficients are adjusted by fitting to the measurements of Devi et al. [65]. What is done differently here is that the adjustment of the potential is made by fitting the half-widths, their temperature dependence, and the line shifts simultaneously. The hope is that only a single set of coefficients will fit all three parameters, constraining the results to the correct potential. The fitting is discussed below.

Wavefunctions and energies must be determined for both CO_2 and N_2. The rotational constant for N_2 was taken as 1.98959 cm^{-1} [84] and the *B*, *D*, and *H* values for CO_2 are from the work of Devi et al. [85,86].

3.1. Initial calculations

3.1.1. Trajectory models

Note, many of the initial calculations used an atom–atom expansion of 8 2 2 to reduce computational time. Calculations of γ and δ for ν_3 band transitions were made using the parabolic trajectory model (PT) of Robert and Bonamy [25] with the isotropic part of the atom–atom potential. These calculations yielded unusual results especially for the line shifts. The agreement with measurement was not good and the results were unphysical. Fig. 1 shows line shifts in units of $cm^{-1}\,atm^{-1}$ versus *m* of the transition (*m* equals –*J* for the P-branch transitions and $J+1$ for the R-branch transitions). Blue x symbols with error bars are the measurements of Devi et al. [87], black triangle symbols are line shifts determined using the parabolic trajectory model. The parabolic trajectory data show unphysical behavior particularly at $m=17$ and for $-24 \le m \le -12$. Generally a smooth variation in the line shift with *m* is observed. The calculations were redone using trajectories determined by solving Hamilton's equations (HE), red circle symbols in Fig. 1, and show the smooth variation. Note, the PT data are shifted to the right and the HE data are shifted to the left by 0.2 to avoid overlapping points. Closer investigation of the calculations employing the parabolic trajectories revealed a large resonance spike in the integrands for both the real and imaginary parts of the integrands. These spikes are shown in Fig. 2 where the real (right panel) and imaginary (left panel) parts of the S_1 and S_2 terms are plotted versus the impact parameter, *b*, in Angstroms. The real and imaginary parts of $S_{2,i2}$ and $S_{2,f2}$ are given by a blue and red dashed dot line respectively, the $S_{2,middle}$ term is the solid black line in the right panel, and the S_1 term is the solid black line in the left panel. Note, the real parts of $S_{2,i2}$ and $S_{2,f2}$ are nearly identical and the lines overlap; the imaginary parts of $S_{2,i2}$ and $S_{2,f2}$ are almost identical and only separate below about 6 Å with $S_{2,i2}$ being slightly larger. At around 6.2 Å we see the real parts of S_2 increase suddenly and the $S_{2,middle}$ part go strongly negative. Similar unphysical behavior occurs for the imaginary terms. This unphysical behavior can be traced to the parabolic trajectories used to determine the resonance functions. When the calculations were redone using trajectories from Hamilton's equations the spikes are removed. One last comment on the PT calculations, when runs are made at slower velocities the calculations sometimes fail due to orbiting collisions, which can lead to a situation

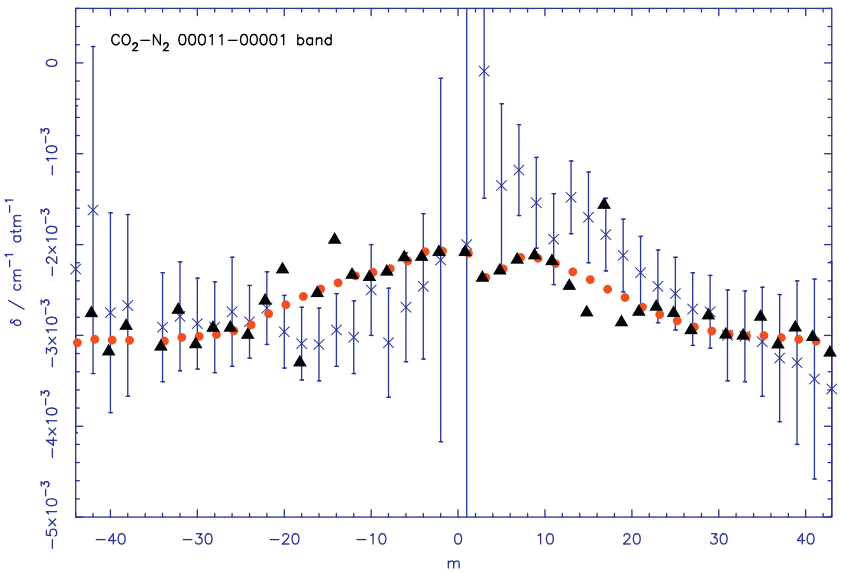

Fig. 1. Measured line shifts for the ν_3 band from Devi et al. [87] (blue x symbols with error bars), CRB calculations using the parabolic approximation for the trajectories (black solid triangle symbols), and CRB calculations solving Hamilton's equations for the trajectories (red solid circle symbols) versus *m*. (For interpretation of the references to color in this figure legend, the reader is referred to the web version of this article.)

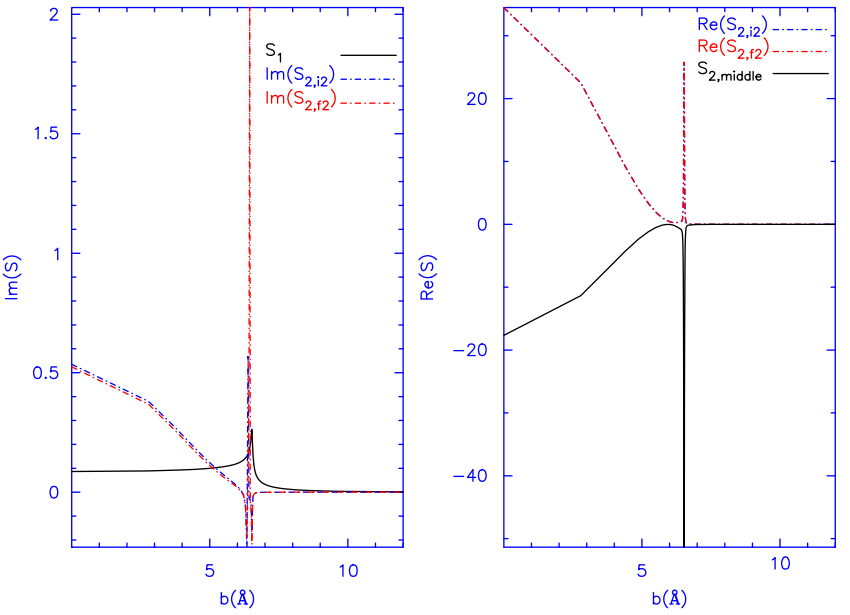

Fig. 2. Real (right panel) and Imaginary (left panel) *outer* and *middle* *S*-matrix components for the P20 line at 100 K versus impact parameter *b* in Angstrom. (For interpretation of the references to color in this figure legend, the reader is referred to the web version of this article.)

where the apparent relative velocity parameter, v'_c in the parabolic trajectory model, becomes negative. While some recent work on using "exact" trajectory models in line shape calculations [43–46] indicates that better results are obtained, here the results indicate that the parabolic model fails to give physical results for CO_2 broadened by N_2. In the calculations that follow the trajectories are determined by solving Hamilton's equations with the potential given by Eq. (4) with the initial Lennard–Jones parameters coming from a least-squares fit to the isotropic parts of the atom–atom potential.

3.1.2. Expansion of the atom–atom potential

Test calculations were made to study the effects of the expansion of atom–atom potential on the half-widths and line shifts. Eighty-two transitions of the ν_3 band were selected and calculations made with the *order* of the atom–atom expansion ranging from 0 (electrostatic) to 22 and *rank* set to 4. Note for *Order* equal to 0, $\ell_1=\ell_2=0$ and for *Order* equal to 2, $\ell_1=\ell_2=2$. Fig. 3 shows the variation of the half-width of the P10 line (upper panel) and line shift of the R16 line (lower panel) at 296 K as a function of the *order* of the expansion of the atom–atom potential. Plots for the other transitions are similar. The percent differences between the half-width for the 22nd *order* calculation and those of *Order*=0 (electrostatic), *Order*=4, and *Order*=16 were determined. For the lines studied, the maximum difference observed for the 0th *Order* calculations was 16%, for the 4th order calculations (the order of the expansion of previous calculations that employed the atom–atom potential) the maximum difference was 12.5%, and for the 16th *Order* calculations the maximum difference was 0.1%. Note, while maximum differences are reported they are the typical values for most of the lines. The percent differences for the line shift reaches ~ -70 comparing with 0th *Order*, just below -50 comparing with 4th *Order*, and to -0.4 comparing to the 16th *Order*. Thus above *Order* 16 the half-width and line shift change little as the order of the potential is increased. To ensure convergence the final calculations of this study were done at 20th *order* and $\ell_1=\ell_2=4$.

Expanding to such high orders should generate many terms in the intermolecular potential. However, CO_2 is a linear triatomic molecule with wavefunctions represented by a single Wigner *D*-matrix, D^J_{00}. When the matrix elements are formed the resulting Racah algebra greatly reduces the number of terms in the intermolecular potential. For example, with the potential expanded to 20 4 4, the CO_2–N_2 system has 210 terms compared with the H_2O–N_2 system which has 1205 terms.

3.1.3. Outer and middle terms

In ATC notation, the second order *S*-matrix can be written in terms of two *outer* terms and one *middle* term [19–21] as shown in Eq. (7). The *middle* term is an elastic contribution $i \leftarrow i$ and $f \leftarrow f$, Eq. (8), the *outer* terms consist of an elastic contribution, $i \leftarrow i$ or $f \leftarrow f$, and a number of inelastic contributions. Because of the symmetry of CO_2 and N_2 the number of inelastic contributions is small. For the *rank* of the intermolecular potential equal to 2 (i.e. quadrupole interactions) there are two terms; one for $\Delta J=2$ and one for $\Delta J=-2$. The total elastic contribution has three contributions: one from the *middle* term, one from the *outer i* and one from the *outer f*. Note, in isotropic Raman *Q* lines the sum of these three elastic terms is zero. Murphy and Boggs [88] developed their "inelastic approximation" based on the assumption that the elastic terms roughly cancel giving calculations involving only the *outer* inelastic terms. Fig. 4, for the R4 transition of CO_2 with $J_2=6$ at 296 K, shows the real parts of $S_{2,f2}$ (in red), $S_{2,i2}$ (in blue) and the $S_{2,middle}$

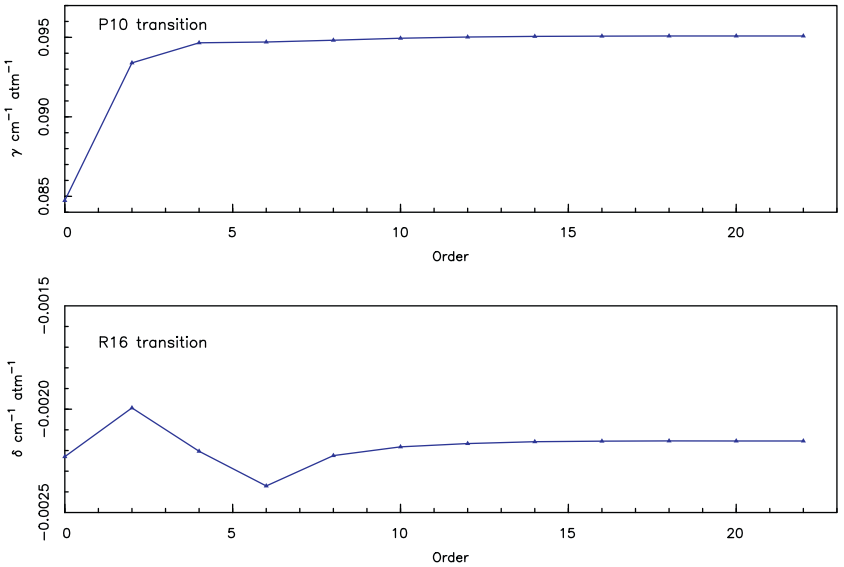

Fig. 3. Convergence of the expansion of the atom–atom potential. Upper panel: half-width in $cm^{-1}\,atm^{-1}$ of the P10 ν_3 transition of CO_2 versus *order* of the atom–atom expansion. Lower panel: line shift in $cm^{-1}\,atm^{-1}$ of the R16 ν_3 transition of CO_2 versus *order* of the atom–atom expansion.

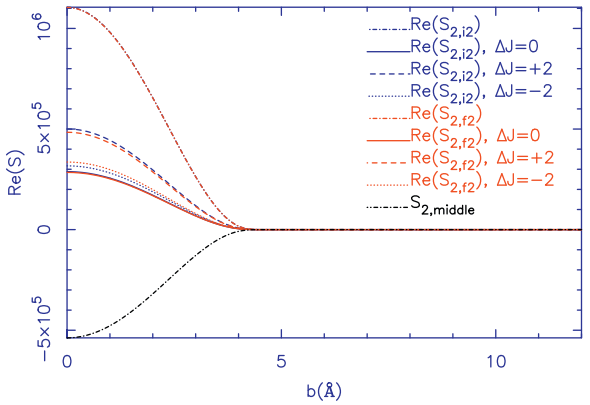

Fig. 4. Components of $Re(S_{2,i2})$, $Re(S_{2,f2})$, and $S_{2,middle}$ versus the impact parameter b in Angstrom for the R4 transition of CO_2 broadened by N_2 at 296 K and $J_2=6$. (For interpretation of the references to color in this figure legend, the reader is referred to the web version of this article.)

term in black versus the impact parameter of the CO_2–N_2 collision pair for a calculation with *rank*=2. The *outer* elastic terms roughly cancel the *middle* (elastic) term, thus for this calculations the optical cross-section would be roughly given by the integral over the *outer i* and *outer f* inelastic terms.

3.2. Parameter adjustment

As stated above, the parameters that enter into the calculation that are not well known are the atom–atom coefficients (Eq. (2)), the coefficients describing the vibrational dependence of the polarizability (Eq. (6)), and the isotropic *L*–*J* parameters needed for the trajectory calculations (Eq. (4)). From calculations made on self-broadening of CO_2 [67] it was found that a quadrupole moment 8% lower than the value reported by Graham et al. [66] is needed to give the proper shape for the half-width and line shift curves as a function of *m*. This value is roughly at the lower error estimate (2σ of the fit plus the systematic error) of the measurements and is discussed in Ref. [67]. The change in the quadrupole moment of CO_2 from the Graham et al. [66] value has almost no effect on the calculated half-widths (1.3% on average) and line shifts (0.3% on average) for the CO_2–N_2 system. The initial atom–atom parameters were determined using the combination rules of Hirschfelder et al. [76] with the homonuclear parameters of Bouanich [89]. These parameters are labeled Pot0 and are presented in Table 1, along with the other parameters that were adjusted.

Table 1
Initial and final adjusted intermolecular potential parameters.

Parameter	Initial value	Final value	% change
$\Theta_{zz}(CO_2)$ (esu)	-4.02×10^{-26}	-3.698×10^{-26}	−8
ε_{ON}/k (K)	43.9	58.69	33.7
ε_{CN}/k (K)	51.28	51.28	0
σ_{ON} (Å)	3.148	3.228	2.5
σ_{CN} (Å)	3.42	3.42	0
ε_{traj}/k (K)	134.325	101.29	−24.6
σ_{traj} (Å)	4.027	3.278	−18.6

To adjust the coefficients describing the vibrational dependence of the polarizability one would need line shift measurements of each of the fundamental bands; ν_1, ν_2, and ν_3. Unfortunately not all the data exist. For $^{12}C^{16}O_2$ there are N_2-induced shift measurements by Thibault et al. [90] for the 00031←00001 band. There are also air-induced shifts for the 00031←00001 band from the work of Toth et al. [91]. Using the Thibault et al. data, CRB calculations of the line shift were made and the a_3 coefficient adjusted to match the measurements. Fig. 5 shows the line shifts calculated with $a_3=0.268$, which gives the best overall fit to the data, versus *m*. The air-induced pressure shifts of Toth

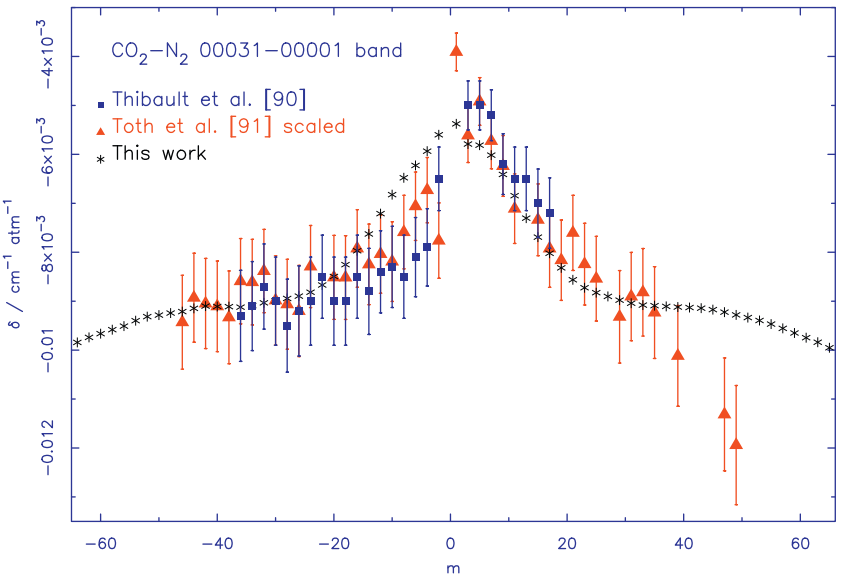

Fig. 5. CO_2–N_2 line shifts for the $3\nu_3$ band from Thibault et al. [90] from Toth et al. [91] (scaled from air induced measurements), and CRB calculated values versus m.

et al. were scaled to N_2 induced pressure shifts using the calculated δ_{air}/δ_{N2} ratios. Using the ratios of the a_1, a_2, and a_3 coefficients determined by Hartmann [83] yields the values $a_1=0.120$ and $a_2=0.0618$. Line shift calculations made for self-broadening of CO_2 [67] yielded a slightly higher value for a_1 when adjusted to fit the shift measurements of Devi et al. [85] and Predoi-Cross et al. [92]. The vibrational dependence of the polarizability is a property of the radiating molecule thus the coefficients should be consistent. Because of this fact, the final choices of the coefficients for the vibrational dependence of the polarizability were taken as $a_1=0.14$, $a_2=0.07$, and $a_3=0.268$ and other intermolecular potential parameters adjusted to fine tune the fit of measured data.

One can also use measurement [80] or *ab initio* data on the dipole polarizability [82,93] to determine the coefficients a_1, a_2, and a_3. As a check, the matrix elements $\langle 00001|\alpha|00001\rangle$, $\langle 10001|\alpha|10001\rangle$, $\langle 10002|\alpha|10002\rangle$, $\langle 00011|\alpha|00011\rangle$, $\langle 00021|\alpha|00021\rangle$, $\langle 00031|\alpha|00031\rangle$ were calculated using data from Tejeda et al. [80] and the fundamentals of CO_2 from HITRAN [1]. The coefficients can be determined from these matrix elements giving $a_1=0.0908$, $a_2=0.0454$, and $a_3=0.1582$, which yield ratios between the coefficients in reasonable agreement with those values determined by fitting the measured data. As outlined above, there exists some uncertainty on the use of the Unsöld approximation for determining the dispersion coefficient $C_6^{0,0}$ [94] and its vibrational dependence. An alternative method, often used, identifies $C_6^{0,0}$ with the L–J constant $4\varepsilon\sigma^6$, while still attributing its vibrational dependence to the polarizability of CO_2. Of course, such a procedure leads to somewhat different values of the a_n parameters: $a_1=0.109$, $a_2=0.0546$, and $a_3=0.209$, in better agreement with the theoretical estimations given above.

The initial trajectory parameters came for fitting the isotropic part of the expanded potential using the Pot0 parameters.

The calculations presented here include determining the temperature dependence of the half-width using the standard power law expression [95]

$$\gamma(T)=\gamma(T_0)\left\{\frac{T_0}{T}\right\}^n \tag{12}$$

where the reference value (T_0) is taken as 296 K. While the calculations were made at 13 temperatures, the determination of n was made using 4 temperatures (200, 250, 296, and 350 K) a range more consistent with the measurements and Earth's atmosphere. Taking the natural logarithm of Eq. (12), linear least-squares fits were made to determine the temperature exponent, n, and the correlation coefficient of the fit for each transition. The uncertainty of the calculated temperature exponents is determined for each transition by using any two of the four calculated points. This generates six 2-point values of n. The maximum difference between the six 2-point values and the least-squares fit value is taken as the uncertainty of the calculation.

CRB calculations of the half-width, its temperature dependence, and the line shift were made for N_2-broadening of $30\,012 \leftarrow 00\,001$ band transitions. The calculations are compared to the measurements of Devi et al. [65]. Note that Devi et al. measured O_2-broadening and using their air-broadening [85] and the standard formula relating air, N_2-, and O_2-broadening for the terrestrial atmosphere, they reported N_2-broadening values as well in Ref. [65]. An example of the initial agreement between the CRB calculations and the measurements is given in Fig. 6. The top panel is the N_2-broadened half-width in $cm^{-1}\,atm^{-1}$ versus m, the middle panel is the N_2-induced line shift in $cm^{-1}\,atm^{-1}$ versus m, and the bottom panel is the temperature dependence of the half-width versus m. There are not many large measured data sets (many m values) for the temperature dependence of the N_2-broadened half-width for this band. The measurements of

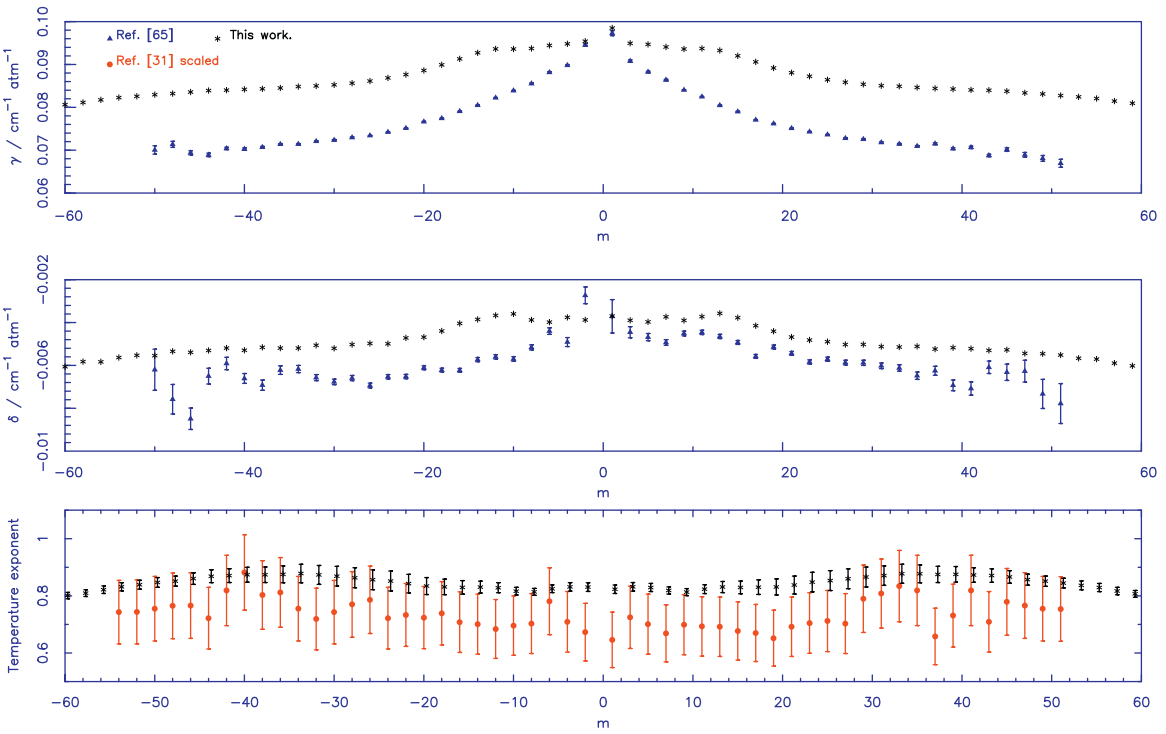

Fig. 6. CO_2-N_2 30012←0001 band: comparison of initial CRB calculations to the measurements of Devi et al. [65] for the half-width and line shift and Predoi-Cross et al. [31] scaled to N_2-broadening for the temperature dependence of the half-width. Top panel half-widths versus m, middle panel line shifts versus m, bottom panel temperature exponent of the half-widths versus m. The calculated temperature exponents also have the error bars from the fit as described in the text.

Valero and Suárez [96] consider values of $|m|$ up to 40 and they report values at 294 and 197 K. However, due to the uncertainty in their half-widths and the small temperature range the resulting temperature exponents have very large error. What is used here are the data of Predoi-Cross et al. [31] for air-broadening scaled to N_2-broadening using the ratio of $n(N_2)$ to n(air) determined from CRB calculations. The agreement between the calculations and the measurements is not very good and the shape of the curve of the calculations does not agree with that of the measured data for any of the parameters.

As described above, the parameters ε_{ON}, σ_{ON}, ε_{CN}, σ_{CN}, ε_{traj}, σ_{traj} need to be adjusted, however, because C is at the center of mass of the CO_2 molecule, the parameters ε_{CN}, σ_{CN} have no effect so only the other 4 are adjusted. The procedure was started with a non-linear least-squares optimization of the parameters, which experienced convergence problems after 12 iterations. Next, CRB calculations were made where each parameter was changed individually by 5% and the percent difference between the iteration 12 results and the adjusted calculation for γ, δ, and n were determined. These data allow the effects of changing each parameter on the half-width, line shift, and temperature dependence of the half-width to be understood. From these data and those in Fig. 6 estimates of how to change the parameters to match the measurement can be made. The determination of the parameters was finished in about 20 iterations by hand. What is found is that the calculated γ, δ, and n are very sensitive to the intermolecular potential parameters. Some parameter sets give good results for the half-widths but poor results for the line shifts or temperature exponents and *vice versa*. Some of these plots are available at the web site of one the authors (faculty.uml.edu/Robert_Gamache). The final coefficients, given in Table 1, give good agreement for all 3 line-shape parameters.

4. Results

Calculations were made at 13 temperatures (75, 80, 90, 100, 125, 150, 200, 250, 296, 350, 400, 500, 700 K) for the 30012←00001 and the 30013←00001 bands for J up to 120. It is difficult to assess the uncertainty of the half-width and line shift calculations. Based on the comparison with measurements the uncertainty of the half-width is estimated to be 1% and the line shifts have an uncertainty of $\pm 0.0007\,cm^{-1}\,atm^{-1}$. The uncertainty in the temperature dependence of the half-width is given for each transition as described above. The calculations for the 30012←00001 and the 30013←00001 bands are identical to within the uncertainty quoted above, i.e. no vibrational dependence of the line shape parameters is observed. The half-widths range from 0.057 to 0.095 $cm^{-1}\,atm^{-1}$, the line shifts are negative and range from -0.0110 to $-0.0044\,cm^{-1}\,atm^{-1}$, and the values of n range from 0.62 to 0.74. The results of the CRB calculations for only the 30012←00001 band are presented in Table 2. However, both calculations are compared with measurement. First we consider the 30012←00001 band data. The agreement with the measurements is shown in

Table 2
Half-width, its temperature dependence, and line shift from the CRB calculations for the CO_2–N_2 system: CO_2 transitions for $-120 \le m \le 121$ in the 30012←00001 band. The half-widths and the line shifts are given in $cm^{-1}\,atm^{-1}$ at $T=296$ K.

m	γ^a	n	δ^a	m	γ^a	n	δ^a
−120	0.0571	0.668 ± 0.068	−0.0108	1	0.0954	0.737 ± 0.014	−0.0044
−118	0.0573	0.664 ± 0.067	−0.0107	3	0.0910	0.737 ± 0.013	−0.0048
−116	0.0576	0.660 ± 0.067	−0.0107	5	0.0897	0.721 ± 0.011	−0.0047
−114	0.0579	0.655 ± 0.065	−0.0106	7	0.0879	0.697 ± 0.008	−0.0049
−112	0.0581	0.652 ± 0.064	−0.0105	9	0.0857	0.674 ± 0.006	−0.0052
−110	0.0584	0.648 ± 0.063	−0.0104	11	0.0835	0.657 ± 0.008	−0.0056
−108	0.0587	0.643 ± 0.062	−0.0103	13	0.0814	0.649 ± 0.011	−0.0059
−106	0.0590	0.639 ± 0.060	−0.0102	15	0.0793	0.647 ± 0.016	−0.0062
−104	0.0594	0.635 ± 0.058	−0.0101	17	0.0775	0.650 ± 0.021	−0.0065
−102	0.0597	0.632 ± 0.056	−0.0100	19	0.0759	0.658 ± 0.026	−0.0067
−100	0.0601	0.628 ± 0.053	−0.0099	21	0.0747	0.670 ± 0.031	−0.0068
−98	0.0604	0.625 ± 0.051	−0.0098	23	0.0738	0.682 ± 0.034	−0.0069
−96	0.0608	0.622 ± 0.048	−0.0097	25	0.0730	0.692 ± 0.036	−0.0070
−94	0.0612	0.619 ± 0.045	−0.0096	27	0.0723	0.700 ± 0.035	−0.0071
−92	0.0616	0.617 ± 0.043	−0.0095	29	0.0719	0.706 ± 0.034	−0.0072
−90	0.0620	0.615 ± 0.040	−0.0094	31	0.0716	0.714 ± 0.033	−0.0072
−88	0.0624	0.613 ± 0.037	−0.0093	33	0.0714	0.719 ± 0.032	−0.0073
−86	0.0628	0.612 ± 0.034	−0.0091	35	0.0712	0.721 ± 0.029	−0.0073
−84	0.0633	0.612 ± 0.032	−0.0090	37	0.0710	0.719 ± 0.026	−0.0073
−82	0.0637	0.612 ± 0.029	−0.0089	39	0.0708	0.716 ± 0.023	−0.0073
−80	0.0641	0.613 ± 0.027	−0.0088	41	0.0707	0.714 ± 0.021	−0.0073
−78	0.0646	0.614 ± 0.024	−0.0087	43	0.0706	0.712 ± 0.019	−0.0073
−76	0.0650	0.616 ± 0.021	−0.0086	45	0.0704	0.708 ± 0.017	−0.0074
−74	0.0655	0.619 ± 0.019	−0.0085	47	0.0702	0.701 ± 0.014	−0.0074
−72	0.0659	0.623 ± 0.017	−0.0084	49	0.0700	0.693 ± 0.012	−0.0075
−70	0.0663	0.626 ± 0.015	−0.0083	51	0.0698	0.687 ± 0.011	−0.0075
−68	0.0668	0.631 ± 0.013	−0.0082	53	0.0695	0.682 ± 0.010	−0.0076
−66	0.0672	0.636 ± 0.011	−0.0081	55	0.0693	0.676 ± 0.009	−0.0076
−64	0.0676	0.642 ± 0.010	−0.0080	57	0.0689	0.669 ± 0.009	−0.0077
−62	0.0680	0.648 ± 0.009	−0.0079	59	0.0686	0.661 ± 0.010	−0.0078
−60	0.0683	0.654 ± 0.008	−0.0078	61	0.0682	0.654 ± 0.010	−0.0079
−58	0.0687	0.661 ± 0.008	−0.0077	63	0.0679	0.649 ± 0.011	−0.0079
−56	0.0690	0.668 ± 0.008	−0.0077	65	0.0675	0.644 ± 0.012	−0.0081
−54	0.0693	0.676 ± 0.008	−0.0076	67	0.0671	0.639 ± 0.014	−0.0082
−52	0.0696	0.682 ± 0.009	−0.0075	69	0.0666	0.633 ± 0.015	−0.0083
−50	0.0698	0.688 ± 0.011	−0.0075	71	0.0662	0.629 ± 0.017	−0.0084
−48	0.0700	0.695 ± 0.012	−0.0074	73	0.0658	0.626 ± 0.019	−0.0085
−46	0.0703	0.703 ± 0.015	−0.0074	75	0.0654	0.623 ± 0.021	−0.0086
−44	0.0705	0.709 ± 0.017	−0.0074	77	0.0650	0.621 ± 0.024	−0.0087
−42	0.0706	0.713 ± 0.019	−0.0073	79	0.0645	0.619 ± 0.026	−0.0088
−40	0.0708	0.715 ± 0.022	−0.0073	81	0.0640	0.617 ± 0.029	−0.0090
−38	0.0709	0.718 ± 0.024	−0.0073	83	0.0636	0.617 ± 0.031	−0.0091
−36	0.0711	0.720 ± 0.028	−0.0073	85	0.0632	0.617 ± 0.033	−0.0092
−34	0.0713	0.720 ± 0.031	−0.0073	87	0.0628	0.618 ± 0.036	−0.0093
−32	0.0715	0.717 ± 0.033	−0.0072	89	0.0623	0.619 ± 0.039	−0.0094
−30	0.0717	0.710 ± 0.034	−0.0072	91	0.0619	0.620 ± 0.042	−0.0095
−28	0.0721	0.703 ± 0.035	−0.0072	93	0.0615	0.622 ± 0.045	−0.0097
−26	0.0726	0.696 ± 0.036	−0.0071	95	0.0612	0.625 ± 0.047	−0.0098
−24	0.0734	0.688 ± 0.035	−0.0070	97	0.0608	0.627 ± 0.050	−0.0099
−22	0.0742	0.676 ± 0.033	−0.0069	99	0.0604	0.630 ± 0.052	−0.0100
−20	0.0753	0.664 ± 0.029	−0.0068	101	0.0600	0.633 ± 0.054	−0.0101
−18	0.0767	0.653 ± 0.023	−0.0067	103	0.0597	0.637 ± 0.057	−0.0102
−16	0.0784	0.648 ± 0.018	−0.0065	105	0.0594	0.641 ± 0.059	−0.0103
−14	0.0804	0.648 ± 0.013	−0.0062	107	0.0591	0.645 ± 0.060	−0.0104
−12	0.0824	0.652 ± 0.009	−0.0059	109	0.0587	0.649 ± 0.062	−0.0105
−10	0.0846	0.665 ± 0.006	−0.0056	111	0.0585	0.653 ± 0.064	−0.0106
−8	0.0868	0.686 ± 0.007	−0.0053	113	0.0582	0.657 ± 0.065	−0.0107
−6	0.0889	0.711 ± 0.009	−0.0051	115	0.0579	0.662 ± 0.066	−0.0108
−4	0.0904	0.731 ± 0.012	−0.0049	117	0.0576	0.666 ± 0.067	−0.0109
−2	0.0918	0.739 ± 0.014	−0.0046	119	0.0574	0.670 ± 0.068	−0.0110
				121	0.0572	0.674 ± 0.069	−0.0110

[a] In units of $cm^{-1}\,atm^{-1}$.

Fig. 7 (same format as Fig. 6). The calculations are compared to the measurements of Devi et al. [65], Li et al. [97], Valero and Suárez [96], and De Rosa et al. [98]. As noted above, the N_2-broadening data of Devi et al. are derived from their air- and O_2-broadening data. Plotted for the temperature dependence, bottom panel, are the air-broadened CRB calculations

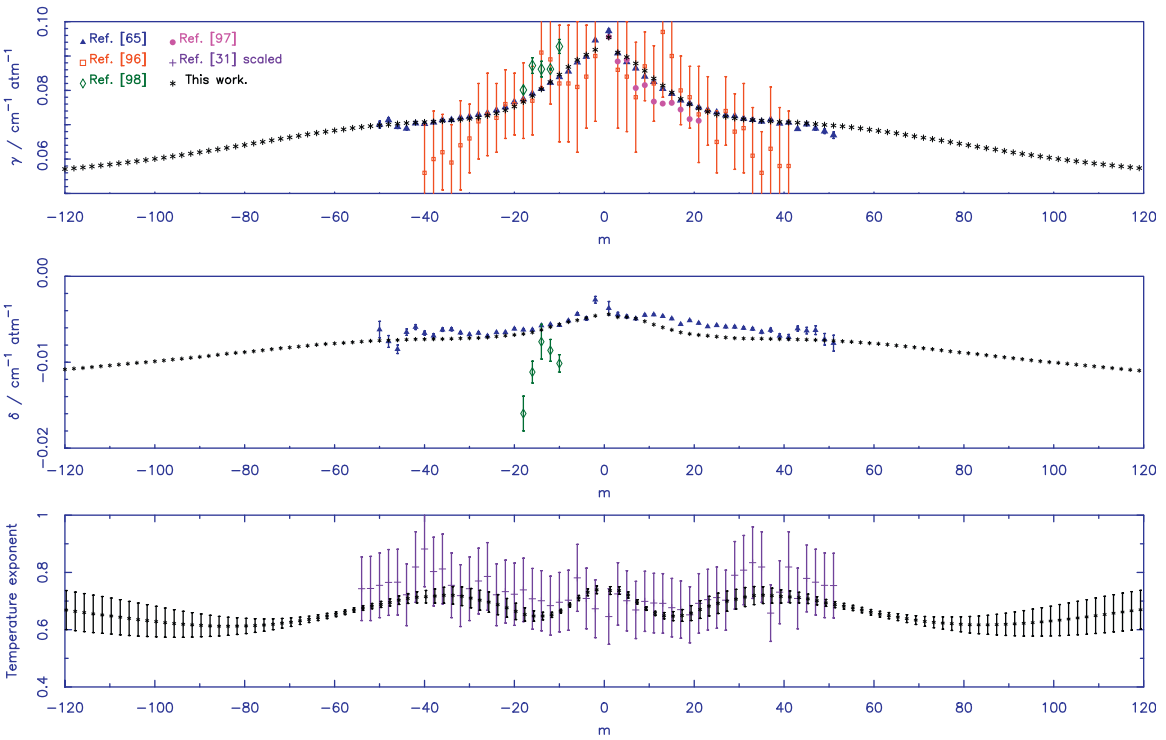

Fig. 7. Final CRB calculations at 296 K for transitions in the 30012←00001 band of CO_2 broadened by N_2 and the measurements (see text for a description) versus m. Top panel half-widths versus m, middle panel line shifts versus m, bottom panel temperature exponent of the half-widths versus m.

and the measurements of Predoi-Cross et al. [31] scaled to N_2-broadening using the air to N_2 ratio from calculations. As noted above, the data of Valero and Suárez [96] are not plotted in the bottom panel, however, the statistics for comparing with their data is included in the analysis.

The average errors and standard deviations of the comparison of calculation to measurement are given in Table 3. The data of Devi et al. [65] are the most complete and considered among the most accurate. Here the calculations of the half-widths show excellent agreement with the 51 measured data: −0.16 average percent difference (APD) and a standard deviation of 1.34%. Because of the magnitude of the line shifts the average deviation between measurement and calculation, $AD = \Sigma_{i=1}^{N}(\delta_{meas} - \delta_{calc})/N$, is presented rather than the percent difference. Also presented for the shifts is the standard deviation of the AD, $S\tilde{D}$. The line shift calculations show good agreement with the measurements as well: 0.00070 cm^{-1} atm^{-1} average deviation with $S\tilde{D} = 0.00057\,cm^{-1}\,atm^{-1}$. The calculations fail to reproduce the asymmetry with respect to m that is seen in the measured data. The calculated temperature exponents are compared with the 53 scaled measurements of Predoi-Cross et al. giving 4.86 APD with a standard deviation of 6.29%. Moreover, the shapes of the curves agree with the measurements. Table 3 shows very good agreement with the half-width data of Li et al. the SD for the comparison with the half-width data of De Rosa et al. is good but their data seem shifted up from the calculations and the other measurements as well. Comparison of the half-width data with Valero and Suárez is good but their data is spread around the calculations and the other measurements. For the line shifts,

Table 3
Statistics for the comparison of the calculations to measurement.

Parameter	Reference	# Data	Average percent difference	Standard deviation in percent
30012←00001				
γ	[65]	51	−0.16	1.34
	[97]	11	−4.47	2.88
	[96]	40	−5.62	10.19
	[98]	5	6.87	2.60
n	[96]	40	−41.29	53.98
	[31][a]	53	4.86	6.29
	Reference	# Data	AD[b]	$S\tilde{D}$ [b]
δ	[65]	51	0.00070	0.00057
	[98]	5	−0.0045	0.0030
	Reference	# Data	APD	SD [b]
30013←00001				
γ	[65]	51	−0.04	1.33
	[101]	15	−0.21	2.03
	[102]	10	−4.73	3.28
	[100]	5	−14.13	1.01
	[99]	24	−2.95	9.59
n	[99]	21	18.19	277.8
	[101]	2	7.60	
	[31][a]	54	5.58	5.18
	Reference	# Data	AD[b]	$S\tilde{D}$ [b]
δ	[65]	49	0.00077	0.00068

[a] Scaled from air-broadening—see text.
[b] See text for definition of AD and $S\tilde{D}$.

the 5 lines measured by De Rosa et al. show poor agreement with the data of Devi et al. and the calculations. As stated above the temperature exponent data from Valero and Suárez show poor agreement with the calculations.

The effect of the imaginary terms on the half-width were studied by making a calculation using only the real components of Robert–Bonamy theory (RRB) and comparing them with the CRB calculations. These calculations were done for the transitions studied above and the average and maximum percent differences between the CRB and RRB data determined. In Fig. 8 the average percent difference and the maximum percent difference are plotted versus the temperature for which the calculations were made. At 296 K the average difference is about one percent and the maximum difference is about 3%. It is evident from Fig. 8 that the inclusion of the imaginary terms will affect the calculation of the temperature dependence of the half-width. This fact implies that calculations made using only the real components, which is what was done in all previous calculations of half-widths for CO_2, will lead to different values for the temperature dependence of the half-width. Given the needs of modern satellite remote sensing programs, calculations of the half-width and its temperature dependence for CO_2 must take into account the imaginary components of the scattering matrices in the formalism.

Calculations of the half-width, its temperature dependence, and the line shift were also made for the 30013←00001 band of CO_2 in collision with N_2. These data are compared with the measurements of Devi et al. [65], Suárez and Valero [99], Pouchet et al. [100], Nakamichi et al. [101], and Hikida and Yamada [102]. Fig. 9 plots these data as in Fig. 7. The statistics for the comparison of measurement and calculations are given in Table 3. Considering the work of Devi et al. for 51 transitions the comparison of the half-widths gives an average percent difference of −0.04 with a standard deviation of 1.33%. The comparison of the 49 line shifts gives $AD=0.00077\,cm^{-1}\,atm^{-1}$ with $S\tilde{D}=0.00068\,cm^{-1}\,atm^{-1}$. Comparing with the cavity-ring-down measurements of Nakamichi et al. gives −0.21 APD with a standard deviation of 2.03% for the 15 transitions studied. It should be noted that the agreement of the data of Nakamichi et al. and Devi et al. is very good. The calculations do not compare as well with the 10 transitions measured by diode laser in the work of Hikida and Yamada; −4.73 APD with a standard deviation of 3.28%. However, Hikida and Yamada chose to fit their spectra with a Galatry profile rather than a Voigt profile. Most studies comparing Galatry and Voigt profiles show the Galatry half-widths are a few percent higher [103]. The results of Hikida and Yamada are a few percent below those of Devi et al., Nakamichi et al., and the CRB calculations (see Fig. 9). The data of Pouchet et al. do not agree with the calculations or the other measurements. The data of Suárez and Valero show considerable scatter around the calculations and the other measured data.

For the temperature dependence Suárez and Valero [99] have made their measurements at 197 and 294 K. Using their data, the temperature dependence of the half-widths can be determined. However, the error on the reported half-widths and the temperature range of the study lead to very large errors in the temperature exponents, so they were not plotted in Fig. 9, but the comparison with the calculations is presented in Table 3. Nakamichi et al. [101] report temperature exponents for the R0 and P8 transitions, which agree well with the CRB calculations: 7.60 APD.

5. Summary

Half-widths, their temperature dependence, and line shifts for transitions from $J=0$ to 120 in 30012←00001 and 30013←00001 bands of CO_2 were calculated using the Complex Robert–Bonamy formalism. It was demonstrated

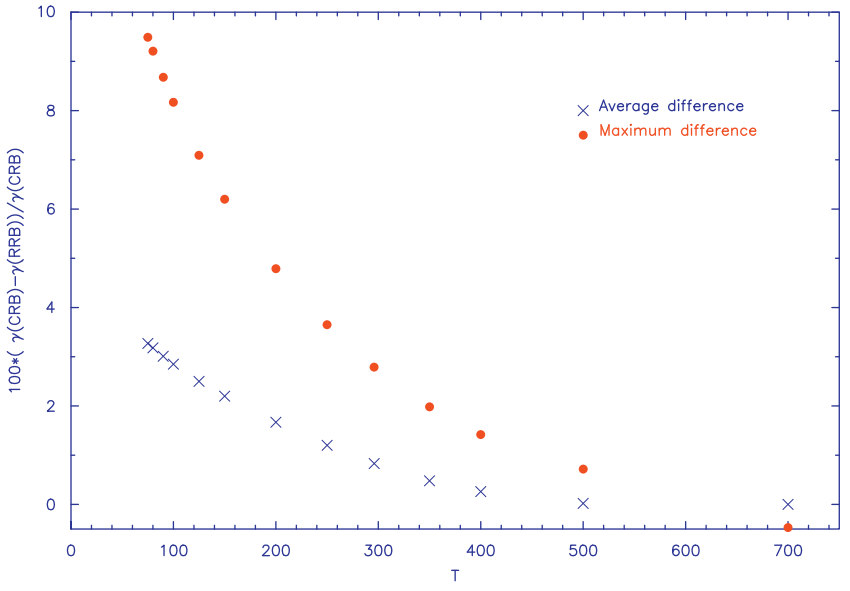

Fig. 8. Effect of the imaginary terms: Average percent difference (CRB-RRB) and maximum percent difference for the transitions in the 30012←00001 band versus temperature in K.

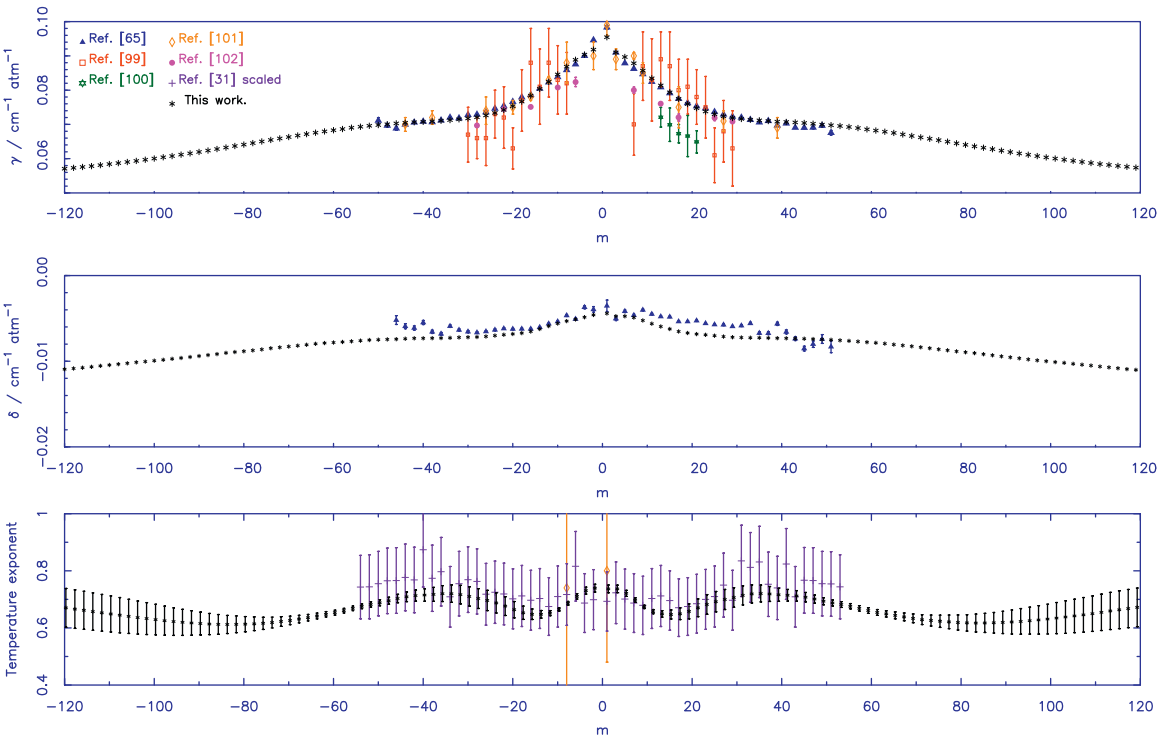

Fig. 9. Final CRB calculations at 296 K for transitions in the 30013←00001 band of CO_2 broadened by N_2 and the measurements (see text for a description) versus m. Top panel half-widths versus m, middle panel line shifts versus m, bottom panel temperature exponent of the half-widths versus m.

that the line shape parameters are very sensitive to the choice of the intermolecular potential, the order of the atom–atom expansion, and the dynamics used in the calculations. Many interesting features were observed for CO_2 as the radiating molecule, which helps explain why previous calculations needed to scale parameters to produce reasonable results. The results indicate (1) the calculations must use Hamilton's Eqs. to determine the trajectories, (2) the intermolecular potential must be expanded to very high *order* and *rank* and (3) the imaginary terms must be included. The parameters describing the intermolecular potential were adjusted to match measurements on the 30012←00001 band for all 3 line shape parameters simultaneously. The calculations made using the final intermolecular potential parameters show excellent agreement with measurements for both of the Fermi-tetrad bands studied in this work. In conclusion, it was found that the use of a single intermolecular potential in CRB calculations can produce half-widths, their temperature dependence, and line shifts that agree very well with measurements.

Acknowledgements

Some of the authors (R.R.G., J.L., A.L.L.) are pleased to acknowledge support of this research by the National Science Foundation through Grant no. ATM-0803135. Any opinions, findings, and conclusions or recommendations expressed in this material are those of the author(s) and do not necessarily reflect the views of the National Science Foundation. R.R.G. and J.M.H. are also grateful to the Paris-Est *Pôle de Recherche et d'Enseignement Supérieur* who provided a one month research scientist position for RRG at LISA in June 2011.

Appendix A. Supplementary materials

Supplementary data associated with this article can be found in the online version at doi:10.1016/j.jqsrt.2012.02.014.

References

[1] Rothman LS, Gordon IE, Barbe A, Benner DC, Bernath PF, Birk M, et al. The HITRAN 2008 molecular spectroscopic database. J Quant Spectrosc Radiat Transfer 2009;110:533–72.
[2] Keeling CD. Variations in concentration and isotopic abundances of atmospheric carbon dioxide. In: Proceedings of the conference on recent research in climatology, Committee on Research in Water Resources and University of California, Scripps Institution of Oceanography, La Jolla, CA, 1957.
[3] Keeling CD. The concentration and isotopic abundances of carbon dioxide in the atmosphere. Tellus 1960;12:200–3.
[4] Lorius C, Jouzel J, Ritz C, Merlivat L, Barkov NI, Korotkevich YS. A 150,000-year climate record from Antartic ice. Nature 1985;316:591–6.
[5] Petit JR, Jouzel J, Raynaud D, Barkov NI, Barnola J-M, Basile I. Climate and atmospheric history of the past 420,000 years from the Vostok ice core. Nature 1999;399:429–36.
[6] IPCC. Climate Change 2007: the physical science basis. Contribution of working Group I to the fourth assessment report of the Intergovernmental Panel on Climate Change, 2007.

[7] Aumann HH, Gregorich D, Gaiser S. AIRS hyper-spectral measurements for climate research: carbon dioxide and nitrous oxide effects. Geophys Res Lett 2005;32:L05806.

[8] Parkinson CL. Aqua: an earth-observing satellite mission to examine water and other climate variables. IEEE Trans Geosci Remote Sens 2003;41:173–83.

[9] Chalon G, Cayla F, Diebel D. IASI: an advance sounder for operational meteorology. In: Proceedings of the 52nd congress of IAF, 2001.

[10] Kramer HJ. Observation of the earth and its environment-survey of missions and sensors. Springer Verlag; 2002.

[11] Inoue G, Yokota T, Oguma H, Higurashi A, Morino I, T. Aoki. Overview of Greenhouse Gases Observing Satellite (GOSAT) of Japan, AGU 2004 fall meeting, 2004.

[12] Crisp D, Atlas RM, Breon F-M, Brown LR, Burrows JP, Ciais P, et al. The orbiting carbon observatory (OCO) mission. Adv Space Res 2004;34:700–9.

[13] Lamouroux J, Tran H, Laraia AL, Gamache RR, Rothman LS, Gordon IE, et al. Updated database plus software for line-mixing in CO_2 infrared spectra and their test using laboratory spectra in the 1.5–2.3 μm region. J Quant Spectrosc Radiat Transfer 2010;111:2321–31.

[14] Rothman LS, Gordon IE, Barber RJ, Dothe H, Gamache RR, Goldman A, et al. HITEMP, the high-temperature molecular spectroscopic database. J Quant Spectros Radiat Transfer 2010;111:2139–50.

[15] Barbe A. Workshop proceedings, atmospheric spectroscopy applications workshop, ASA REIMS 96, 1996.

[16] Smith MAH, editor. NASA conference publication 2396, NASA, 1985.

[17] Smith MAH, editor. Third Langley spectroscopic Parameters workshop, NASA Langley Research Center, 1992.

[18] Yamamoto G, Tanaka M, Aoki T. Estimation of rotational line widths of carbon dioxide bands. J Quant Spectrosc Radiat Transfer 1969;9:371–82.

[19] Anderson PW. Dissertation. Physics, Harvard University; 1949.

[20] Anderson PW. Pressure broadening in the microwave and infrared regions. Phys Rev 1949;76:647–61.

[21] Tsao CJ, Curnutte B. Line-widths of pressure-broadened spectral lines. J Quant Spectrosc Radiat Transfer 1962;2:41–91.

[22] Bouanich J-P, Brodbeck C. Contribution des moments octupolaire et hexadecapolaire a l'elargissement des raies spectrales de molecules lineaires. J Quant Spectrosc Radiat Transfer 1974;14:141–51.

[23] Bykov AD, Lavrentieva NN, Sinitsa LN. Calculation of CO_2 broadening and shift coefficients for high-temperature databases. Atmos Ocean Opt 2000;13:1015–9.

[24] Arié E, Lacome N, Arcas P, Levy A. Oxygen- and air-broadened linewidths of CO_2. Appl Opt 1986;25:2584–91.

[25] Robert D, Bonamy J. Short range force effects in semiclassical molecular line broadening calculations. J Phys France 1979;40:923–43.

[26] Margottin-Maclou M, Dahoo P, Henry A, Valentin A, Henry L. Self-, N_2-, and O_2-broadening parameters in the ν_3 and $\nu_1+\nu_3$ bands of $^{12}C^{16}O_2$. J Mol Spectrosc 1988;131:21–35.

[27] Rosenmann L, Hartmann J-M, Perrin MY, Taine J. Collisional broadening of CO_2 IR lines. II. Calculations. J Chem Phys 1988;88:2999–3006.

[28] Rosenmann L, Perrin MY, Hartmann J-M, Taine J. Diode-laser measurements and calculations of CO_2-line-broadening by H_2O from 416 to 805 K and by N_2 from 296 to 803 K. J Quant Spectrosc Radiat Transfer 1988;40:569–76.

[29] Rosenmann L, Hartmann J-M, Perrin MY, Taine J. Accurate calculated tabulations of IR and Raman CO_2 line broadening by CO_2, H_2O, N_2, O_2 in the 300–2400-K temperature range. Appl Opt 1988;27:3902–7.

[30] Gamache RR, Rosenmann L. N_2-, O_2-, air-, and self broadening of CO_2 transitions and temperature dependence for HITRAN, Unpublished work, University of Massachusetts Lowell, 1992.

[31] Predoi-Cross A, McKellar ARW, Benner DC, Devi VM, Gamache RR, Miller CE, et al. Temperature dependences for air-broadened Lorentz half-width and pressure shift coefficients in the 30013←00001 and 30012←00001 bands of CO_2 near 1600 nm. Can J Phys 2009;87:517–35.

[32] Kubo R. Generalized cumulant expansion method. J Phys Soc Japan 1962;17:1100–20.

[33] Lynch R. Half-widths and line shifts of water vapor perturbed by both nitrogen and oxygen. PhD dissertation, Physics Department, University of Massachusetts, Lowell, 1995.

[34] Lynch R, Gamache RR, Neshyba SP. Fully complex implementation of the Robert–Bonamy formalism: halfwidths and line shifts of H_2O broadened by N_2. J Chem Phys 1996;105:5711–21.

[35] Lynch R, Gamache RR, Neshyba SP. N_2 and O_2 induced halfwidths and line shifts of water vapor transitions in the (301)←(000) and (221)←(000) bands. J Quant Spectrosc Radiat Transfer 1998;59:595–613.

[36] Gamache RR, Lynch R, Plateaux JJ, Barbe A. Halfwidths and line shifts of water vapor broadened by CO_2: measurements and complex Robert–Bonamy formalism calculations. J Quant Spectrosc Radiat Transfer 1997;57:485–96.

[37] Gamache RR, Lynch R, Neshyba SP. New developments in the theory of pressure-broadening and pressure-shifting of spectral lines of H_2O: the complex Robert–Bonamy formalism. J Quant Spectrosc Radiat Transfer 1998;59:319–35.

[38] Lynch R, Gamache RR, Neshyba SP. Pressure broadening of H_2O in the (301)←(000) Band: effects of angular momentum and close intermolecular interactions. J Quant Spectrosc Radiat Transfer 1998;59:615–26.

[39] Labani B, Bonamy J, Robert D, Hartmann J-M, Taine J. Collisional broadening of rotation-vibration lines for asymmetric top molecules I. Theoretical model for both distant and close collisions. J Chem Phys 1986;84:4256–67.

[40] Hartmann J-M, Taine J, Bonamy J, Labani B, Robert D. Collisional broadening of rotation-vibration lines for asymmetric-top molecules II. H_2O diode laser measurements in the 400–900 K range; calculations in the 300–2000 K range. J Chem Phys 1987;86:144–56.

[41] Ma Q, Tipping RH, Gamache RR. Uncertainties associated with theoretically calculated N_2-broadened half-widths of H_2O lines. Mol Phys 2010;108:2225–52.

[42] Gamache RR, Laraia AL, Lamouroux J. Half-widths, their temperature dependence, and line shifts for the HDO-CO_2 system for applications to planetary atmospheres. Icarus 2011;213:720–30.

[43] Buldyreva J, Bonamy J, Robert D. Semiclassical calculations with exact trajectory for N_2 rovibrational Raman linewidths at temperatures below 300 K. J Quant Spectrosc Radiat Transfer 1999;62:321–43.

[44] Buldyreva J, Benec'h S, Chrysos M. Infrared nitrogen-perturbed NO linewidths in a temperature range of atmospheric interest: an extension of the exact trajectory model. Phys Rev A 2000;63:012708.

[45] Ma Q, Tipping RH, Boulet C, Thibault F, Bonamy J. Vibration-dependent trajectories and their effects on vibrational dephasing. J Mol Spectrosc 2007;243:105–12.

[46] Lamouroux J, Gamache RR, Laraia AL, Ma Q, Tipping RH. Comparison of trajectory models in calculations of N_2-broadened half-widths and N_2-induced line shifts for the rotational band of $H_2^{16}O$ and comparison with measurements, in press, this issue (doi:10.1016/j.jqsrt.2011.11.010) J Quant Spectrosc Radiat Transfer.

[47] Kolb AC, Griem H. Theory of line broadening in multiplet spectra. Phys Rev 1958;111:514–21.

[48] Baranger M. Simplified quantum-mechanical theory of pressure broadening. Phys Rev 1958;111:481–93.

[49] Griem HR. Classical radiation theory. Mc Graw Hill; 1964.

[50] Leavitt RP, Korff D. Cut-off-free theory of impact broadening and shifting in microwave and infrared gas spectra. J Chem Phys 1981;74:2180–98.

[51] Looney JP, Herman RM. Air broadening of the hydrogen halide-I. N_2-broadening and shifting in the HCl fundamental. J Quant Spectrosc Radiat Transfer 1987;37:547–57.

[52] Jones JE. On the determination of molecular fields.II. From the equation of state of a gas. Proc R Soc A 1924;106:463–77.

[53] Hartmann J-M, Camy-Peyret C, Flaud J-M, Bonamy J, Robert D. New accurate calculations of ozone line-broadening by O_2 and N_2. J Quant Spectrosc Radiat Transfer 1988;40:489–95.

[54] Neshyba SP, Lynch R, Gamache RR, Gabard T, Champion J-P. Pressure induced widths and shifts for the ν_3 band of methane. J Chem Phys 1994;101:9412–21.

[55] Antony B, Gamache P, Szembek C, Niles D, Gamache RR. Modified complex Robert–Bonamy formalism calculations for strong to weak interacting systems. Mol Phys 2006;104:2791–9.

[56] Oka T. Advances in atomic and molecular physics. New York: Academic Press; 1973.

[57] Ben-Reuven A. Spectral line shapes in gases in the binary-collision approximation, Adv Chem Phys. In: Prigogine I and Rice SA, editors. Academic Press: New York. 1975. p. 235.

[58] Neshyba SP, Gamache RR. Improved line broadening coefficients for asymmetric rotor molecules: application to ozone perturbed by nitrogen. J Quant Spectrosc Radiat Transfer 1993;50:443–53.

[59] Gray CG, Gubbins KE. Theory of molecular fluids. Oxford: Clarendon Press; 1984.

[60] Gray CG. On the theory of multipole interactions. Can J Phys 1968;46:135–9.

[61] Sack RA. Two-center expansion for the powers of the distance between two points. J Math Phys 1964;5:260–8.
[62] Downs J, Gray CG, Gubbins KE, Murad S. Spherical harmonic expansion of the intermolecular site-site potential. Mol Phys 1979;37:129–40.
[63] Luo Y, Agren H, Vahtras O, Jorgensen P, Spirko V, Hettema H. Frequency-dependent polarizabilities and first hyperpolarizabilities of H_2O. J Chem Phys 1993;98:7159–64.
[64] Toth RA, Brown LR, Miller CE, Malathy Devi V, Benner DC. Spectroscopic database of CO_2 line parameters: 4300–7000 cm^{-1}. J Quant Spectrosc Radiat Transfer 2008;109:906–21.
[65] Devi VM, Benner DC, Miller CE, Predoi-Cross A. Lorentz half-width, pressure-induced shift and speed-dependent coefficients in oxygen-broadened CO_2 bands at 6227 and 6348 cm^{-1} using a constrained multispectrum analysis. J Quant Spectrosc Radiat Transfer 2010;111:2355–69.
[66] Graham C, Pierrus J, Raab RE. Measurements of the electric quadrupole moments of CO_2, CO and N_2. Mol Phys 1989;67:939–55.
[67] Lamouroux J, Gamache RR, Laraia AL, Hartmann J-M, Boulet C. Semiclassical calculations of half-widths and line shifts for transitions in the 30012←00001 and 30013←00001 bands of CO_2 III: self collisions. J Quant Spectrosc Radiat Transfer, submitted for publication.
[68] Bose TK, Cole RH. Dielectric and pressure virial coefficients of imperfect gases. II. CO_2–argon mixtures. J Chem Phys 1970;52:140–7.
[69] Tanaka Y, Jursa AS, LeBlanc FJ. Higher ionization potentials of linear triatomic molecules. I. CO_2. J Chem Phys 1960;32:1199–205.
[70] Mulder F, van Dijk G, van der Avoird A. Multipole moments, polarizabilities and anisotropic long range interaction coefficients for N_2. Mol Phys 1980;39:407–25.
[71] Bogaard MP, Orr BJ. In: Buckingham AD, editor, MPT international review of science, physical chemistry, series two, vol. 2. Molecular structure and properties, 1975. London: Butterworths [chapter 5].
[72] Lofthus A. The molecular spectrum of nitrogen, Department of Physics, University of Oslo, Blindern, Norway, Spectroscopic report no. 2, vol. 1, 1960.
[73] Diaz Pena M, Pando C, Renuncio JAR. Combination rules for intermolecular potential parameters. I. Rules based on approximations for the long-range dispersion energy. J Chem Phys 1982;76:325–32.
[74] Diaz Pena M, Pando C, Renuncio JAR. Combination rules for intermolecular potential parameters. II. Rules based on approximations for the long-range dispersion energy and an atomic distortion model for the repulsive interactions. J Chem Phys 1982;76:333–9.
[75] Good RJ, Hope CJ. Test of combining rules for intermolecular distances. potential function constants from second virial coefficients. J Chem Phys 1971;55:111–6.
[76] Hirschfelder JO, Curtiss CF, Bird RB. Molecular theory of gases and liquids. New York: Wiley; 1964.
[77] Gamache RR, Fischer J. Half-widths of $H_2^{16}O$, $H_2^{18}O$, $H_2^{17}O$, $HD^{16}O$, and $D_2^{16}O$: I comparison between isotopomers. J Quant Spectrosc Radiat Transfer 2003;78:289–304.
[78] Gamache RR. Line Shape parameters for water vapor in the 3.2 to 17.76 mm region for atmospheric applications. J Mol Spectrosc 2005;229:9–18.
[79] Gamache RR, Hartmann J-M. Collisional parameters of H_2O lines: effects of vibration. J Quant Spectrosc Radiat Transfer 2004;83:119–47.
[80] Tejeda G, Maté B, Montero S. Overtone Raman spectrum and molecular polarizability surface of CO_2. J Chem Phys 1995;103:568–76.
[81] Chrysos M, Verzhbitskiy IA, Rachet F, Kouzov AP. The isotropic remnant of the CO_2 near-fully depolarized Raman $2\nu_3$ overtone. J Chem Phys 2011;134:104310.
[82] Haskopoulos A, Maroulis G. Dipole and quadrupole (hyper)polarizability for the asymmetric stretching of carbon dioxide: Improved agreement between theory and experiment. Chem Phys Lett 2006;417:235–40.
[83] Hartmann J-M. A simple empirical model for the collisional spectral shift of air-broadened CO_2 lines. J Quant Spectrosc Radiat Transfer 2009;110:2019–26.
[84] Huber KP, Herzberg G. Molecular spectra and molecular structure: constants of diatomic molecules. New York: Van Nostrand; 1979.
[85] Devi VM, Benner DC, Brown LR, Miller CE, Toth RA. Line mixing and speed dependence in CO_2 at 6348 cm^{-1}: Positions, intensities, and air- and self-broadening derived with constrained multispectrum analysis. J Mol Spectrosc 2007;242:90–117.
[86] Devi VM, Benner DC, Brown LR, Miller CE, Toth RA. Line mixing and speed dependence in CO_2 at 6227.9 cm^{-1}: Constrained multispectrum analysis of intensities and line shapes in the 30013←00001 band. J Mol Spectrosc 2007;245:52–80.
[87] Devi VM, Benner DC, Smith MAH, Rinsland CP. Nitrogen broadening and shift coefficients in the 4.2–4.5-μm bands of CO_2. J Quant Spectrosc Radiat Transfer 2003;76:289–307.
[88] Murphy JS, Boggs JE. Collision broadening of rotational absorption lines. I. Theoretical formulation. J Chem Phys 1967;47:691–702.
[89] Bouanich J-P. Site-site Lennard–Jones potential parameters for N_2, O_2, H_2, CO and CO_2. J Quant Spectrosc Radiat Transfer 1992;47:243–50.
[90] Thibault F, Boissoles J, Le Doueen R, Bouanich JP, Areas P, Boulet C. Pressure induced shifts of CO_2 lines: measurements in the $00^{0}3$–$00^{0}0$ band and theoretical analysis. J Chem Phys 1992;96:4945–53.
[91] Toth RA, Miller CE, Devi VM, Benner DC, Brown LR. Air-broadened halfwidth and pressure shift coefficients of $^{12}C^{16}O_2$ bands: 4750–7000 cm^{-1}. J Mol Spectrosc 2007;246:133–57.
[92] Predoi-Cross A, Unni AV, Liu W, Schofield I, Holladay C, McKellar ARW, Hurtmans D. Line shape parameters measurement and computations for self-broadened carbon dioxide transitions in the 30012←00001 and 30013←00001 bands, line mixing, and speed dependence. J Mol Spectrosc 2007;245:34–51.
[93] Maroulis G. Electric (hyper)polarizability derivatives for the symmetric stretching of carbon dioxide. Chem Phys 2003;291:81–95.
[94] Mulder F, Thomas GF, Meatha WJ. A critical study of some methods for evaluating the C 6, C 8 and C 10 isotropic dispersion energy coefficients using the first row hydrides, CO, CO_2 and N_2O as models. Mol Phys 1980;41:249–69.
[95] Birnbaum G. Microwave pressure broadening and its application to intermolecular forces. Adv Chem Phys 1967;12:487–548.
[96] Valero FPJ, Suárez CB. Measurement at different temperatures of absolute intensities, line half-widths, and broadening by Ar and N_2 for the $30^{0}1_{II}$←$00^{0}0$ band of CO_2. J Quant Spectrosc Radiat Transfer 1978;19:579–90.
[97] Li JS, Liu K, Zhang WJ, Chen WD, Gao XM. Self-, N_2- and O_2-broadening coefficients for the $^{12}C^{16}O_2$ transitions near-IR measured by a diode laser photoacoustic spectrometer. J Mol Spectrosc 2008;252:9–16.
[98] De Rosa M, Corsi C, Gabrysch M, D'Amato F. Collisional broadening and shift of lines in the $2\nu_1+2\nu_2+\nu_3$ band of CO_2. J Quant Spectrosc Radiat Transfer 1999;61:97–104.
[99] Suárez CB, Valero FPJ. Intensities, self-broadening, and broadening by Ar and N_2 for the 301_{III}←000 band of CO_2 measured at different temperatures. J Mol Spectrosc 1978;71:46–63.
[100] Pouchet I, Zéninari V, Parvitte B, Durry G. Diode laser spectroscopy of CO_2 in the 1.6 μm region for the in situ sensing of the middle atmosphere. J Quant Spectrosc Radiat Transfer 2004;83:619–28.
[101] Nakamichi S, Kawaguchi Y, Fukuda H, Enami S, Hashimoto S, Kawasaki M, et al. Buffer-gas pressure broadening for the $(3\ 0^{0}1)_{III}$←$(0\ 0\ 0)$ band of CO_2 measured with continuous-wave cavity ring-down spectroscopy. Phys Chem Chem Phys 2006;8:364–8.
[102] Hikida T, Yamada KMT. N_2- and O_2-broadening of CO_2 for the $(30^{0}1)_{III}$←$(00^{0}0)$ band at 6231 cm^{-1}. J Mol Spectrosc 2006;239:154–9.
[103] Hartmann J-M, Boulet C, Robert D. Collisional effects on molecular spectra: laboratory experiments and models, consequences for applications. Amsterdam: Elsevier Science; 2008.